
06 Mar 2023

NaGaSe₂: A Water-Loving Multifunctional Non-Van Der Waals Layered Selenogallate

Srikanth Balijapelly

Santhoshkumar Sundaramoorthy

Dibya Jyoti Mondal

Sanjit Konar

et. al. For a complete list of authors, see https://scholarsmine.mst.edu/phys_facwork/2264

Follow this and additional works at: https://scholarsmine.mst.edu/phys_facwork

 Part of the [Physics Commons](#)

Recommended Citation

S. Balijapelly et al., "NaGaSe₂: A Water-Loving Multifunctional Non-Van Der Waals Layered Selenogallate," *Inorganic Chemistry*, vol. 62, no. 9, pp. 3886 - 3895, American Chemical Society, Mar 2023. The definitive version is available at <https://doi.org/10.1021/acs.inorgchem.2c04237>

This Article - Journal is brought to you for free and open access by Scholars' Mine. It has been accepted for inclusion in Physics Faculty Research & Creative Works by an authorized administrator of Scholars' Mine. This work is protected by U. S. Copyright Law. Unauthorized use including reproduction for redistribution requires the permission of the copyright holder. For more information, please contact scholarsmine@mst.edu.

NaGaSe₂: A Water-Loving Multifunctional Non-van der Waals Layered Selenogallate

Srikanth Balijapelly,[†] Santhoshkumar Sundaramoorthy,[†] Dibya Jyoti Mondal, Sanjit Konar, Nikolay Gerasimchuk, Aleksandr Chernatynskiy, and Amitava Choudhury*



Cite This: *Inorg. Chem.* 2023, 62, 3886–3895



Read Online

ACCESS |



Metrics & More

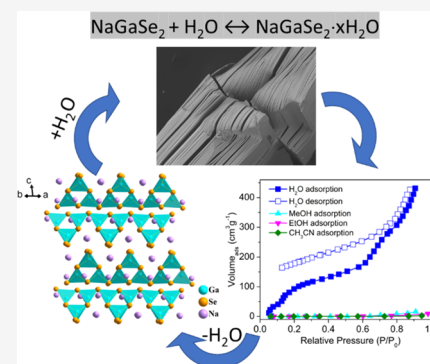


Article Recommendations



Supporting Information

ABSTRACT: A missing member of well-known ternary chalcometallates, a sodium selenogallate, NaGaSe₂, has been synthesized by employing a polyselenide flux and stoichiometric reaction. Crystal structure analysis using X-ray diffraction techniques reveals that it contains supertetrahedral adamantane-type Ga₄Se₁₀ secondary building units. These Ga₄Se₁₀ secondary building units are further connected via corners to form two-dimensional (2D) [GaSe₂]_∞⁻ layers stacked along the *c*-axis of the unit cell, and the Na ions reside in the interlayer space. The compound has an unusual ability to absorb water molecules from the atmosphere or a nonanhydrous solvent to form distinct hydrated phases, NaGaSe₂·*x*H₂O (where *x* can be 1 and 2), with an expanded interlayer space, as verified by X-ray diffraction (XRD), thermogravimetric–differential scanning calorimetry (TG-DSC), desorption, and Fourier transform infrared spectroscopy (FT-IR) studies. The in situ thermodiffraction indicates the emergence of an anhydrous phase before 300 °C with the decrease of interlayer spacings and reverting to the hydrated phase within a minute of re-exposure to the environment, supporting the reversibility of such a process. Structural transformation induced through water absorption results in an increase of Na ionic conductivity by 2 orders of magnitude compared to that of the pristine anhydrous phase, as verified by impedance spectroscopy. Na ions from NaGaSe₂ can be exchanged in the solid-state route with other alkali and alkaline earth metals in a topotactic or nontopotactic way, leading to 2D isostructural and three-dimensional networks, respectively. Optical band gap measurements show a band gap of ~3 eV for the hydrated phase, NaGaSe₂·*x*H₂O, which is in good agreement with the calculated band gap using a density functional theory (DFT)-based method. Sorption studies further confirm the selective absorption of water over MeOH, EtOH, and CH₃CN with a maximum water uptake of 6 molecules/formula unit at a relative pressure, *P*/*P*₀, of 0.9.



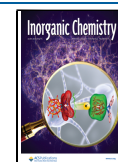
INTRODUCTION

Hydration–dehydration plays an important role in altering the fundamental physical properties of solids, especially in alkali metal-containing non-van der Waals (non-vdW) 2D materials.^{1–4} Non-vdW solids containing Li and Na ions have the propensity to intercalate water due to the high enthalpy of hydration of these two alkali ions.⁵ As a consequence of this hydration–dehydration, often, the individual layers restack reversibly or there is an increase in the interlayer distances or complete exfoliation of layers, leading to changes in the properties.^{6–8} These property changes can be as exotic as the change of superconducting transition temperature (*T*_C) and more common phenomena as the change of ionic conductivity of the interlayer alkali ions as a function of hydration.^{3,9} Note that the incorporated water molecules into the crystal structure especially into the oxide framework may undergo dissociation, leading to enhancement of proton ion conduction.^{7,10,11} Recently, Lotsch's, zur Loye's, and our groups have found that such hydration–dehydration phenomena are more prevalent in Li- and Na-intercalated layered chalcogenides, which in addition to showing some interesting properties also

possess challenges in crystal structure determination of both hydrated and dehydrated phases as a result of the stacking fault and preferred orientations.^{4,8,12–14} Lotsch's group has demonstrated the impact of hydration on Li-ion conductivity,¹² while our group has demonstrated that in NaGaS₂, Na-ion conductivity increases many times in the hydrated phase.¹⁴ In addition to ionic conductivity, the ability of selective absorption of water from solution and vapor makes NaGaS₂ a unique material that can selectively trap water from the atmosphere and in a mixture of solvents. On the other hand, zur Loye's group has demonstrated the ion exchange capability of NaGaS₂ and the dynamic role of hydration.¹³ Recently, zur Loye's group also demonstrated reversible water uptake in Na-intercalated layered actinide chalcogenides.¹⁵ With this

Received: November 30, 2022

Published: February 20, 2023



renewed interest in the hydration–dehydration behavior of alkali ion-containing non-vdW layered chalcogenide materials and considering the fact that most of the superionic Na- and Li-ion conductors are from the chalcogenide family,^{16–19} it is important to study their hydration chemistry and their effect on properties. However, such studies are limited to sulfide families. We, therefore, sought to extend this study to the selenide family. Our first objective was to examine whether a selenide analogue of NaGaS₂ exists and if so, does it have the same characteristics of water absorption properties and more importantly can this water absorption property be utilized for some application. Herein, we report the first successful synthesis of NaGaSe₂, its crystal structure, preliminary ion-exchange property, Na-ion conductivity in hydrated and anhydrous phases, and its selective water vapor uptake property. In addition, we also report the experimental band gap and theoretical band structure of this wide band gap semiconductor.

EXPERIMENTAL SECTION

Synthesis. NaGaSe₂ was synthesized both by stoichiometric and flux reactions between Ga and Na₂Se or Na₂Se₃ flux, respectively. For the stoichiometric reaction, 0.5 mM Na₂Se, 1 mM Ga shavings, and 1.5 mM elemental Se were mixed together and transferred into carbon-coated quartz ampoules. In the case of the flux route, first, the Na₂Se₃ flux was synthesized by taking stoichiometric amounts of Na and Se in liquid NH₃ following Birch reduction techniques.²⁰ Shavings from the Ga ingot and Na₂Se₃ powders were mixed in 2:3 molar ratio and loaded into a carbon-coated quartz ampoule. All chemical loadings were performed in an argon-filled glovebox (O₂ < 2 ppm). The reactants were sealed under vacuum using a flame torch. The ampoules were heated up to 750 °C at a rate of 35 °C/h and kept at that temperature for 4 days for stoichiometry and 5 days for flux-based reactions followed by cooling to room temperature at a rate of 35 °C/h. Plate-shaped, colorless shiny crystals (100% yield with respect to Ga) were observed from both syntheses. The product from the flux reactions was washed several times with *N,N*-dimethylformamide (DMF) to remove the remaining polyselenide flux. The crystals were found to be reasonably stable under ambient conditions; however, they absorb moisture through intercalation and swell through interlayer expansion as the sulfide analogue.¹⁴ On prolonged exposure (more than 10 days), they tend to lose long-range ordering with a high degree of water intercalation and surface oxidation (discussed later). A picture showing the as-synthesized DMF-washed crystals is provided in Figure S1. The source of absorbed moisture can be the nonanhydrous DMF used in washing excess flux and air. It was extremely challenging to get a good-quality crystal for single-crystal X-ray structure solution. However, after several efforts, it was possible to get a thin single crystal from a quick one-cycle DMF-washed sample that led to successful solution of the crystal structure. Although large crystals appeared nice in bare eyes, under a microscope, there were visible cracks, and on stroking with a needle, they were exfoliating like mica sheets instead of breaking. The stoichiometric reaction product did not require a DMF wash; however, it still absorbs water with momentary exposure during the crystal selection for single-crystal study, and we could not find a good-quality single-crystal. Also, note that flux-growth crystals have better quality with respect to single-crystal characteristics, but the downside is that they need to be washed with DMF, promoting the possibility of water intercalation. The rest of the samples were ground into fine powder inside a glovebox for characterization and property studies.

X-ray Crystallography. The crystal structure was solved by introducing a disordered model where two Se and two sodium atoms were split due to elongated thermal ellipsoids. The details are given in the Supporting Information. Crystal data and the refinement parameters are given in Table 1, and atomic coordinates, isotropic, and anisotropic thermal parameters are supplied in the Supporting

Table 1. Crystal Data and Refinement Details of NaGaSe₂

empirical formula	NaGaSe ₂
formula weight	250.63
temperature	298(2) K
wavelength	0.71073 Å
crystal system	monoclinic
space group	C2/c
unit cell dimensions	$a = 10.738(3)$ Å, $b = 10.750(3)$ Å, $c = 14.152(4)$ Å, $\beta = 100.954(5)^\circ$
volume	1603.8(8) Å ³
Z	16
density (calculated)	4.152 mg/m ³
absorption coefficient	24.876 mm ⁻¹
goodness-of-fit on F^2	1.114
final R indices [$I > 2\sigma(I)$]	0.051
R indices (all data)	0.1382

Information (Tables S1 and S2). The selected bond lengths are given in Tables 2 and S3.

Table 2. Ga–Se Bond Lengths in NaGaSe₂

moiety	distances (Å)	moiety	distances (Å)
Ga1–Se2	2.396(3)	Ga2–Se4	2.395(3)
Ga1–Se4	2.399(2)	Ga2–Se5	2.396(3)
Ga1–Se1A	2.404(4)	Ga2–Se1 ^a	2.405(4)
Ga1–Se1	2.408(4)	Ga2–Se1A ^a	2.405(4)
Ga1–Se3A	2.413(5)	Ga2–Se3 ^b	2.415(6)
Ga1–Se3	2.416(5)	Ga2–Se3A ^b	2.419(5)

^a– x , y , $-z + 1/2$. ^b– $x + 1/2$, $y + 1/2$, $-z + 1/2$.

Powder X-ray Diffraction. The flux route-synthesized DMF-washed sample was finely ground in air for lab-PXRD data collection (blue trace in Figure 1). Since the stoichiometric reaction did not

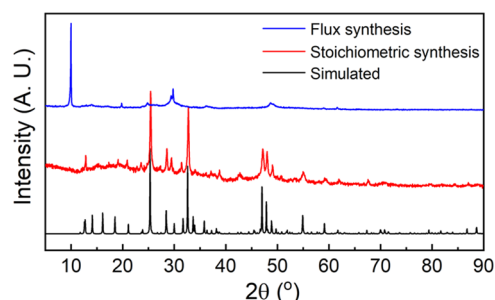


Figure 1. Comparison of simulated and laboratory-grade ($\lambda = 1.5405$ Å) experimental powder patterns with stoichiometrically synthesized and flux route-synthesized, hand-ground NaGaSe₂.

require DMF washing, the as-synthesized sample was handled throughout inside an Ar-filled glovebox and taken out in an airtight cell for laboratory-grade PXRD of the anhydrous phase as shown in Figure 1. High-resolution synchrotron PXRD (S-PXRD) data were collected on hand-ground DMF-washed powder samples, which were handled in air, however, transferred to an Ar-filled glovebox, and sealed in a quartz capillary. To obtain S-PXRD data of the anhydrous phase, the sample was heated at 300 °C for 12 h under vacuum and transferred to an Ar-filled glovebox (O₂ and H₂O < 0.2 ppm) without exposing to air and then sealed in a quartz capillary. The temperature of dehydration was decided from the thermogravimetric analysis (TGA), which showed that water removal was complete around ~300–350 °C (discussed later). Figure 2a shows the comparison of

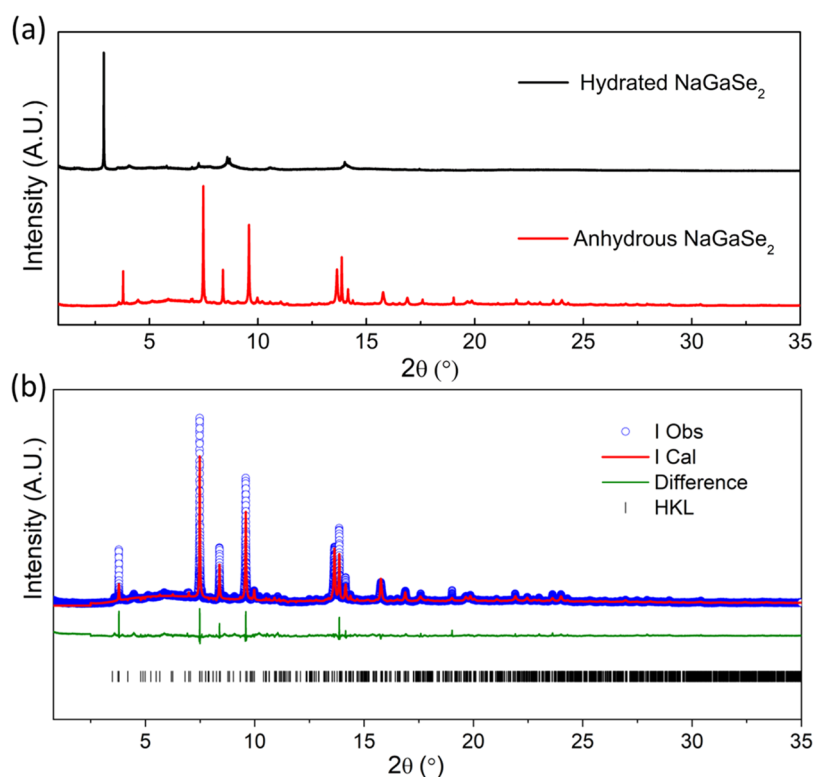


Figure 2. (a) Comparison of synchrotron PXRD ($\lambda = 0.457920 \text{ \AA}$) of hydrated NaGaSe_2 ($d = 9.06 \text{ \AA}$ phase) from flux route DMF-washed samples and anhydrous NaGaSe_2 ($\lambda = 0.458102 \text{ \AA}$) obtained by dehydrating the above-mentioned sample and (b) Rietveld refinement on the synchrotron PXRD ($\lambda = 0.458102 \text{ \AA}$) pattern of anhydrous NaGaSe_2 .

S-PXRD data of both hydrated and anhydrous phases derived from the flux synthesis. Our attempt to solve the structure of the hydrated phase was not successful because of the presence of the preferred orientation and stacking faults resulting in missing lines and broadened peaks, which posed difficulty in accurate indexing of diffraction lines. However, we have been able to perform Rietveld refinement of the anhydrous phase from the S-PXRD to the extent that we can reliably say that the anhydrous phase is indeed NaGaSe_2 . For the Rietveld refinement, nondisordered atomic coordinates were used. The refinement converged to a reasonably low value of R_w (Table S4), although the difference curve has the signature of preferred orientation and severe intensity mismatch (Figure 2b). In addition, some diffraction lines are missing or display poor intensity due to stacking faults. The unit cell, atomic coordinates, and isothermal parameters were refined without restraints. The refined unit cell parameters are close to the single-crystal X-ray structure solution, and the bond length distribution is within the limits of sum of cation and anion ionic radii (compare Tables 2, S3, and S5). The thermal parameter refinement of atoms indicated higher thermal parameters for Se1 and Se3, which were split for the single-crystal solution (compare Tables S1 and S6). In addition to these, we have carried out in situ thermodiffraction in an inert gas flow and also performed ex situ time-dependent PXRD, the details of which are given in the Supporting Information.

TGA–DSC Analysis. The as-synthesized, DMF-washed crystals and momentarily exposed stoichiometrically synthesized samples were used to record simultaneous TG/DSC traces on a TA Instrument Q-600 (Delaware) in an alumina crucible in the range between 30 and 1050 °C under a pure nitrogen flow at $100 \pm 1 \text{ mL/min}$ and a heating rate of 10 °C/min. The brand-new crucible was calcined prior to each experiment using a propane torch to remove moisture.

IR Spectroscopy. The IR spectrum was collected using a Thermo Nicolet iS50 FT-IR spectrometer over 400–4000 cm^{-1} on the air-exposed sample using the ATR mode.

SEM Analysis. The SEM images were taken with a Hitachi TM1000 tabletop scanning electron microscope on the as-synthesized NaGaSe_2 crystals.

Diffuse Reflectance Spectral Study. The diffuse reflectance spectrum of the powdered sample of air-exposed hydrated NaGaSe_2 was characterized at room temperature using an Agilent Cary 5000 UV–Vis–NIR spectrophotometer equipped with a Praying mantis attachment using BaSO_4 as a white background reference. The absorption spectrum was derived from reflectance data by converting into the Kubelka–Munk function $\alpha/S = (1 - R)^2/2R$, where α is the absorption coefficient, S is the scattering coefficient, and R is the reflectance.²¹

Impedance Studies. AC impedance measurements were performed on a Biologic Instruments SP-150 impedance analyzer with an AC signal amplitude of 500 mV in a frequency range of 1 Hz–1 MHz. Inside an argon-filled glovebox ($\text{O}_2 < 0.1 \text{ ppm}$) ~80 mg of the DMF-washed hand-ground powder sample was cold-pressed by applying 280 MPa vertical force in a stainless-steel pressing die. Indium foil was used for the blocking electrodes on both sides of the pellet and placed in an airtight Swagelok-type cell. To measure the temperature dependence of ionic conductivity, the Swagelok cell was placed inside a temperature-controlled box furnace. The impedance data were collected at every 10 °C increase, and the temperature was held constant for at least an hour at each temperature to reach thermal equilibrium and achieve a steady state. To measure the impedance data on the anhydrous sample, the sample was vacuum-heated at 300 °C to remove the water molecules. Similar measurement protocol was used for the anhydrous sample.

DFT Band Structure Calculations. The electronic band structure was calculated on the un-disordered model of NaGaSe_2 using density functional theory (DFT) as incorporated in the Vienna *Ab initio* simulation package (VASP).^{22–25} To get the correct band structure and most accurate band gap, hybrid functional (HSE06)²⁶ calculations were performed. The kinetic energy cutoff was set to 520 eV, and a Monkhorst–Pack k -point grid size of $2 \times 2 \times 2$ was used for Brillouin zone integration.²⁷ A fully relaxed atomic structure using the

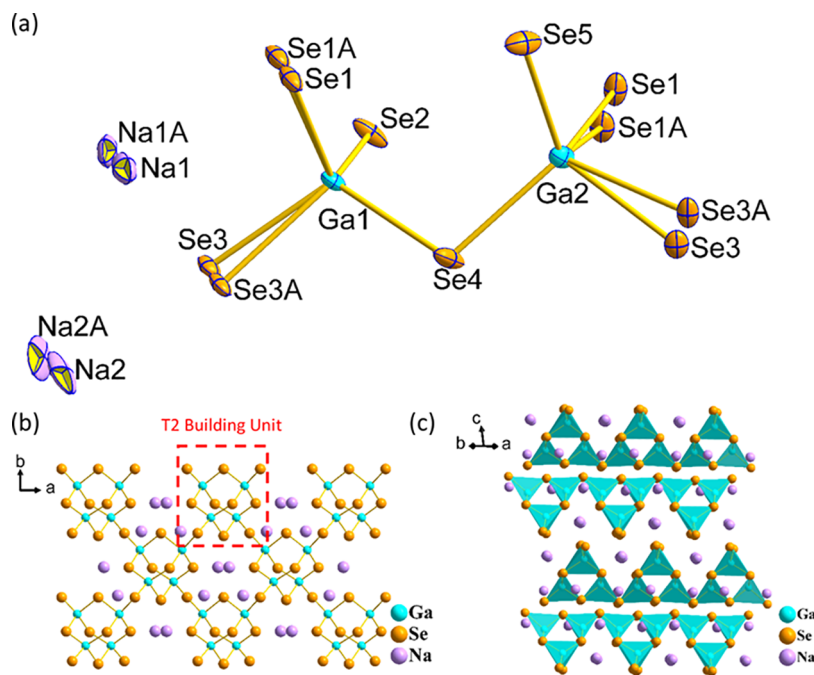


Figure 3. (a) Asymmetric unit of NaGaSe₂ showing the split position of atoms. Thermal ellipsoids are given at 50% probability. (b) Single 2D layer of [GaSe₂]⁻ along the *ab* plane; (c) Stacking of the [GaSe₂]⁻ layers in NaGaSe₂. Note that for (b) and (c), the disordered atoms are not shown for clarity of the picture.

standard DFT method was used for further calculations using hybrid functionals. The convergence threshold was set to 10⁻⁶ eV for total energy and 10⁻³ eV/Å for the maximum force employed for relaxation. A Gaussian smearing of 0.1 eV was used for the calculations of the density of states.

Solid-State Ion Exchange. A mixture of anhydrous NaGaSe₂ (20–30 mg) and an excess metal chloride salt (LiCl, KCl, RbCl, and SrCl₂) in 1:5 ratio was hand-ground using a mortar and pestle inside an argon-filled glovebox. The mixture was pelletized using a stainless-steel pressing die and vacuum-sealed in a carbon-coated quartz ampoule. The sealed quartz tube was placed in a temperature-controlled furnace, and the temperature of the furnace was ramped to 500 °C at a rate of 20 °C/h and maintained for 48 h before cooling to room temperature at a rate of 30 °C/h. A relatively higher temperature, although still below the melting points of either the halides or NaGaSe₂, was used. After breaking the ampoule, the pellet was washed with 10% water in DMF to remove the excess salt flux. The insoluble crystalline powder left after washing was vacuum-dried and transferred to an argon-filled glovebox. Unlike NaGaS₂, NaGaSe₂ is sensitive toward water; therefore, aqueous ion exchange was not performed.

Vapor Sorption Study. Vapor sorption studies were performed on the hand-ground powder sample of NaGaSe₂. The sample was dehydrated under vacuum at 250 °C for 10 h in a BELSORP AQUA (BEL JAPAN) volumetric adsorption analyzer before performing small-molecule sorption measurements.

RESULTS AND DISCUSSION

Structure Description. NaGaSe₂ crystallizes in the C2/*c* space group in a TlGaSe₂ structure type²⁸ and is also isostructural to the sulfide analogue, NaGaS₂.¹⁴ It is to be noted that this is the first report of a Na-containing TlGaSe₂ structure type in the Ga–Se family, although isostructural AGaSe₂ for A = K, Rb, and Cs has already been reported in the literature.^{28–35} The asymmetric unit of the crystal structure contains two Ga, two Na, and five Se atoms. Two of the Se atoms (Se1 and Se3) and two Na atoms are modeled as disordered and split into two positions (Figure 3a). The Ga1

atom is surrounded by four Se atoms in a tetrahedral coordination, and four such tetrahedra are corner-shared to form an adamantane-like supertetrahedral building unit, Ga₄Se₁₀, also denoted as T2 unit. These Ga₄Se₁₀ units are further connected to other such units via a bridging Se3 atom extending perpendicular to the [001] direction to form negatively charged undulated layers of [GaSe₂]⁻ (Figure 3b). These stacked layers are separated by the charge-balancing Na ions residing in the valleys formed by the T2 building units along the *ab* plane (Figure 3c). Ga–Se bond distances are in the range of 2.395(2)–2.419(5) Å, which are in good agreement with the isostructural KGaSe₂.³² Na atoms are coordinated with eight Se atoms in a distorted bi-capped trigonal prismatic fashion (6 + 2) with Na–Se bond distances in the range of 2.86(2)–3.52(3) Å (Figure S2).

Water Intercalation and Reversible Restacking. The first impression from the laboratory-grade PXRD data of the flux reaction product is that there is absolutely no match with the simulated PXRD pattern generated from the atomic coordinates of single-crystal X-ray structure solution (Figure 1). The appearance of a high-intensity low-angle line indicates the substantial expansion of the interlayer distance, a situation previously observed in the case of the sulfide analogue NaGaS₂, attributed to water intercalation in the interlayer space.¹⁴ On the other hand, the laboratory PXRD of the stoichiometrically synthesized NaGaSe₂ matches well with the simulated pattern of the anhydrous phase (Figure 1). Also, note that this group of compounds, both sulfide¹⁴ and the selenide analogues, does not yield very good powder patterns. This is due to their mica-like exfoliation during grinding. Rather than forming fine powder, grinding creates more stacking faults. Stacking faults along with the preferred orientation result in poor diffraction patterns with missing lines. This is why in the experimental powder pattern, some lines are absent or poorly exhibited, especially in the 2θ range of 13–19° (Cu Kα). However, there is a very good overall agreement between the as-synthesized

powder pattern from stoichiometric synthesis and the simulated pattern (Figure 1).

Obtaining an anhydrous phase directly from synthesis is possible because the stoichiometric synthesis route does not require washing with DMF to remove the excess flux, thereby offering a direct path to arrive at the anhydrous phase. The zur Loye group also used the solid-state reaction of Ga_2S_3 and Na_2S to produce NaGaS_2 .¹³ While we were preparing our article, we came across a mechanochemical synthesis of NaGaS_2 employing Na_2S and Ga_2S_3 in stoichiometric amounts, which initially forms an amorphous compound and following heat treatment forms crystalline NaGaS_2 .³⁶ Our stoichiometric synthesis employs the selenide analogues of the same reagents. However, it is important to highlight the extreme hydrophilicity of this as-synthesized anhydrous sample. This sample while transferring into the in situ heating chamber absorbs water in the interlayer space within a matter of minute, as evident from the emergence of a low-angle line at $2\theta = 9.75^\circ$ ($d_{\text{spacing}} = 9.06 \text{ \AA}$) (Figure 4). Note that this low-angle line is

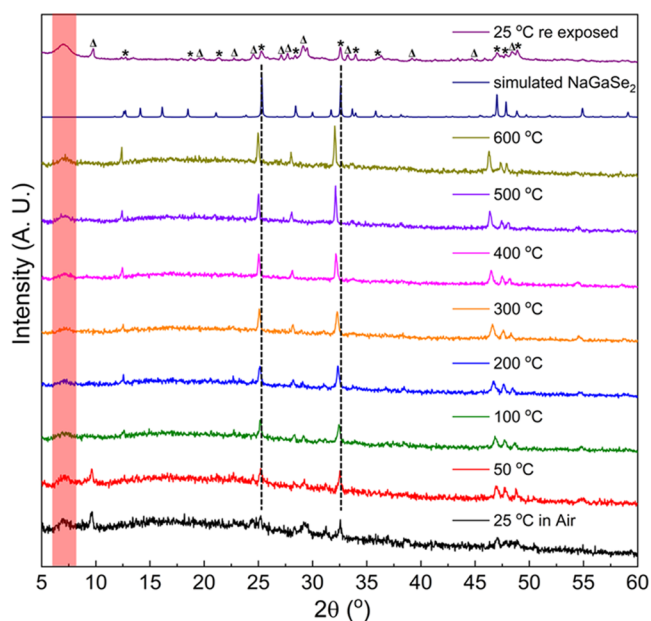


Figure 4. Thermodiffractogram of the stoichiometrically synthesized NaGaSe_2 from room temperature to 600°C exhibiting reversible water absorption without any structural destruction. The low-angle broad peak appears due to the use of the airtight cell.

similar to the hydrated sulfide analogue where it appears at $d = 8.94 \text{ \AA}$, for a stable monohydrate phase, $\text{NaGaS}_2 \cdot \text{H}_2\text{O}$.^{13,14} However, this phase is not fully hydrated, as it is evident from TGA (discussed below), and also, the lines from the anhydrous parent phase are still present. When the sample is heated under a UHP Ar flow with simultaneous PXRD data collection, it quickly transforms into the anhydrous phase above 100°C . The thermodiffractogram does not show any structural transformation at high temperatures (up to 600°C) as also supported by TG-DSC (discussed later) and remains in the monoclinic NaGaSe_2 ($C2/c$) phase (Figure 4). It should be mentioned here that even a smaller number of lines appear in the thermodiffractogram for the anhydrous phase in the laboratory-grade ($\text{Cu K}\alpha$) quick scans due to the severe stacking faults, preferred orientation, and reduced intensities from the use of the airtight Anton Paar cell. Only the most

intense lines show up at 2θ values of 12.83° ($d_{\text{spacing}} = 6.89 \text{ \AA}$), 25.45° ($d_{\text{spacing}} = 3.50 \text{ \AA}$), and 32.74° ($d_{\text{spacing}} = 2.73 \text{ \AA}$) with the cluster of lines between $2\theta = 46$ and 49° . In addition, the lines shift to the left as a function of temperature due to volume expansion. After cooling to room temperature under an Ar flow, it remains in the same phase. The anhydrous sample is then exposed to air; it again reabsorbs water and forms a partially hydrated structure, as evident from the re-emergence of the line at $d = 9.06 \text{ \AA}$ along with lines of the anhydrous phase (Figure 4). Thus, NaGaSe_2 shows a similar reversible restacking behavior as observed in the sulfide analogue NaGaS_2 .¹⁴ A similar thermodiffractogram experiment has been performed with the hydrated sample obtained from the flux-based synthesis route (Figure S3) with the first line at $d = 9.06 \text{ \AA}$ and no diffraction lines from the anhydrous phase. This phase can be assumed as a fully converted monohydrated phase, $\text{NaGaSe}_2 \cdot x\text{H}_2\text{O}$ ($x = 1$), by drawing similarity with NaGaS_2 .^{13,14} The hydrated phase converts to the anhydrous phase upon heating and goes back to a partly hydrated phase on momentary exposure (~ 1 min) and toward a more dominant $d = 9.06 \text{ \AA}$ hydrated phase after 12 h in air, as the anhydrous phase lines further diminish in intensity. Note here that although in the thermodiffractogram, the line intensities are weak for the anhydrous phase and several lines are missing, they can all be recovered upon annealing at 300°C for 12 h under vacuum. This has been shown by the S-PXRD data of the anhydrous phase obtained by dehydrating the flux route-obtained hydrated phase (Figure 2). Furthermore, we have also performed *ex situ* time-dependent rehydration studies, where the partially hydrated phase slowly turns into a $d = 9.06 \text{ \AA}$ hydrated (presumably monohydrate) phase after 1 day (Figure S4). Notably, it slowly transforms into a second hydrated phase over time with further uptake of water and expansion of the interlayer space, as evident from the emergence of a new line at $2\theta = 8.35^\circ$ ($d_{\text{spacing}} = 10.59 \text{ \AA}$) ($\text{Cu K}\alpha$) after 3 days of exposure. On prolonged exposure (~ 10 days), it mostly converts to the second hydrated phase with the most prominent line at $d = 10.59 \text{ \AA}$ (Figure S4). At this point, all lines broaden with partial loss of crystallinity due to the occurrence of severe stacking faults. Simultaneously, surface oxidation also takes place turning the sample color to red due to the presumed formation of amorphous Se, following the reaction $2\text{NaGaSe}_2 + 2\text{O}_2 + \text{H}_2\text{O} = 2\text{NaOH} + \text{Ga}_2\text{O}_3 + 4\text{Se}$. Moisture from air is expected to react with Na_2O to form NaOH .

Simultaneous thermogravimetric and differential scanning calorimetry (TG-DSC) analysis was performed on the as-synthesized DMF-washed crystals of NaGaSe_2 to examine the compositional changes and occurrence of any phase transformation. The TG-DSC plot (Figure 5a) shows a weight loss of $\sim 10.2\%$ from a flux-produced DMF-washed hydrated phase, which corresponds to a loss of ~ 1.6 water molecules per formula unit in the temperature range of 40 – 300°C . The DSC data show that major water loss takes place in two steps at ~ 165 and 210°C below 300°C . After 300°C , the percent weight loss is less than 1% until 500°C , which could be due to the removal of residual water. The broad exothermic peak at $\sim 878.5^\circ\text{C}$ is due to the reaction of a trace amount of O_2 impurity (in the purging gas) with NaGaSe_2 ; the reaction starts at $\sim 750^\circ\text{C}$ and ends at $\sim 975^\circ\text{C}$. The oxidation process is also evident through visual inspection of the sample before and after the TG-DSC study (Figure S5), which clearly shows the formation of a melt-like crust due to the reaction with a change

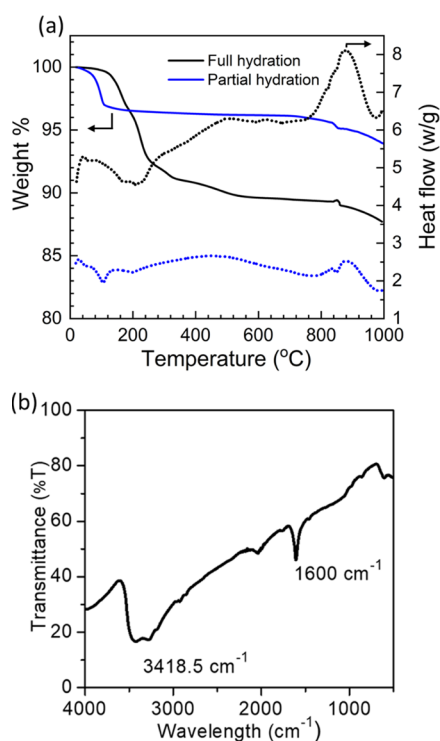


Figure 5. (a) Simultaneous TGA (solid line)–DSC (dotted line) plots of the as-synthesized, DMF-washed (black), and vacuum-dried (40 °C) sample of NaGaSe₂ and partly hydrated NaGaSe₂ (blue) from stoichiometric synthesis and (b) FT-IR spectrum of hydrated DMF-washed NaGaSe₂.

in color due to Se formation ($2\text{NaGaSe}_2 + 2\text{O}_2 = \text{Na}_2\text{O} + \text{Ga}_2\text{O}_3 + 4\text{Se}$). The partially hydrated sample (stoichiometrically synthesized and momentarily exposed, ~ 1 min) shows a very similar TG-DSC trace except that the amount of the absorbed water is only $\sim 3.5\%$ corresponding to $0.5 \text{ H}_2\text{O}$ per formula. However, since the compound is only partially hydrated and if we assume that the $d = 9.06 \text{ \AA}$ line is for monohydrate, only 50% of the sample is hydrated in the partially hydrated phase. This phase loses 100% of water within 100 °C (blue trace in Figure 5a). After that, it has an almost flat line until 850 °C in TGA and displays no sign of phase transition in the DSC curve. After 850 °C, there is evidence of oxidative decomposition from the ppm-level oxygen impurity as the previous sample.

To further confirm the presence of water molecules, FT-IR was performed on the as-synthesized DMF-washed powder samples (Figure 5b). The DMF-washed NaGaSe₂ clearly displays broad vibration absorption bands due to the symmetric (ν_1) and antisymmetric (ν_3)–O–H stretching centered at 3418.5 cm^{-1} and H–O–H bending modes at 1608 cm^{-1} , which are typical IR bands of water. Therefore, the FT-IR study further supports the presence of water molecules in the structure.

In summary, based on the evidence from d -spacings, we can conclude that the water intercalation happens in two steps. It is highly likely that in the first step, it takes up one water molecule per formula unit and forms a somewhat stable structure with the lattice expansion $d = 9.06 \text{ \AA}$ due to a monohydrate ($\text{NaGaSe}_2 \cdot \text{H}_2\text{O}$) phase akin to the $\text{NaGaS}_2 \cdot \text{H}_2\text{O}$ structure.¹⁴ The DFT simulation for the sulfide analogue indicated that the intercalated H_2O coordinates with the Na in two positions in the interlayer space, while Na is still coordinated to the framework S in other four positions. In the case of the $d = 10.59 \text{ \AA}$ phase, we speculate that further expansion of the interlayer space is due to the absorption of a second water molecule making the Na ion fully coordinated with water, satisfying all six coordinations. Such a bilayer formation has been reported in a thiophosphate.² Our TGA data for the flux-based DMF-washed sample show an intermediate value of x , $\text{NaGaSe}_2 \cdot x\text{H}_2\text{O}$ ($x \sim 1.6$), meaning that part of the sample has transitioned from the monohydrate phase by the time TG-DSC was performed.

The SEM images (Figure 6) clearly show evidence of water absorption and subsequent interlayer expansion through cracking along the ab plane, where the layer-like sheets are splitting and separating from each other. The cleavage of layers with the thickness in the range of $5\text{--}10 \mu\text{m}$ is observed in DMF-washed air-exposed large crystals, which also led to substantial swelling. We have also taken SEM images of the samples re-exposed to air from the thermodiffraction study (Figure S6). The texture of the re-exposed samples looks somewhat different. The larger splits are still present, but some of the thin cracks are no longer visible.

It is important to note here that the water absorption is very selective for the Na analogue of the AGaQ_2 ($A = \text{Na, K, Rb, and Cs}$; $Q = \text{S, Se, and Te}$) structure family, which is due to the high enthalpy of hydration of the Na^+ ion and the ability of water to intercalate in the interlayer space, resulting in the expansion of interlayer stacking. LiGaQ_2 , a well-known SHG

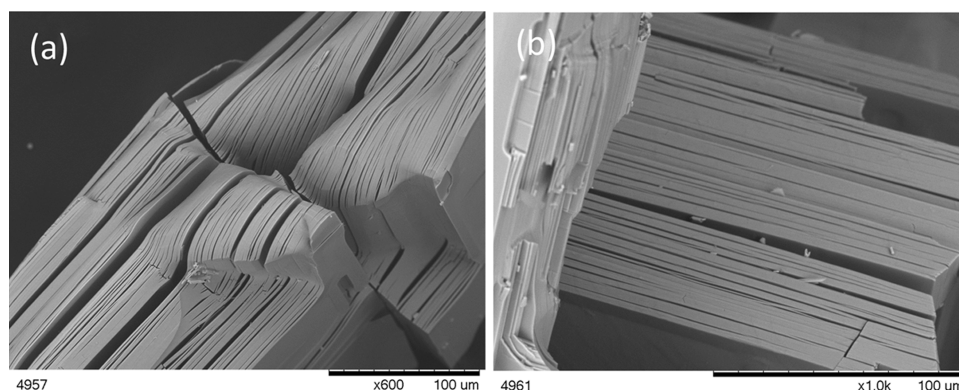


Figure 6. SEM image of the as-synthesized, DMF-washed, and vacuum-dried sample of NaGaSe₂. (a,b) Two different images at different magnifications.

material, forms a different structure type, which is three-dimensional and does not absorb water because of the lack of room for H₂O to enter the structure.^{37,38} However, a recently reported compound, Na₂GaS₂Cl, with an identical layer topology built up of T2 building units as in NaGaQ₂ (Q = S and Se) but with subtle difference in the coordination of interlayer Na ions due to NaCl salt inclusion does not seem to absorb water.³⁹ In this compound, which can be written as NaGaS₂·NaCl, instead of interlayer expansion through water intercalation, NaCl expands the interlayer space and strong ionic interactions between S²⁻ and Cl⁻ with Na⁺ prohibit Na⁺ to be hydrophilic. This implies that the water absorption property is not solely governed by the identity of the alkali ion in the interlayer space but also the anion (S, Se, and Cl) coordination around the alkali ions.³⁹

Optical Band Gap and Band Structure Analysis. To estimate the optical band gap of the hydrated compound, NaGaSe₂·H₂O (flux-synthesized DMF-washed), a DRS study was carried out on the coarsely ground powder sample. A band gap of 3.00 eV is obtained (Figure 7a) after converting the

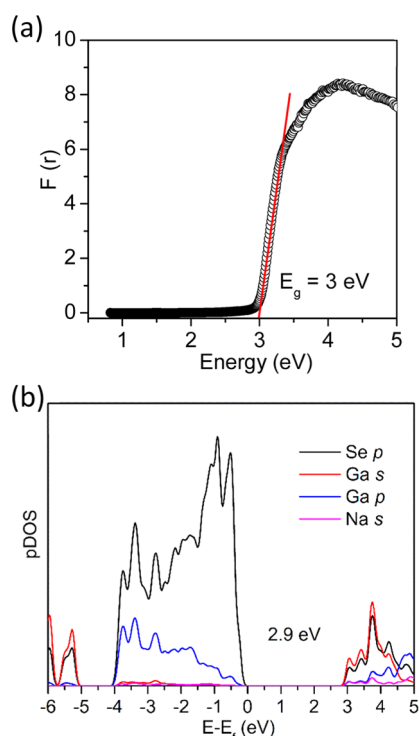


Figure 7. (a) Diffuse reflectance spectra of NaGaSe₂ and (b) calculated electronic band structure of NaGaSe₂ using the hybrid functional (HSE06).

reflectance data into absorbance using the Kubelka–Munk function.²¹ The band gap measurement of the anhydrous material could not be performed, as the material is highly moisture-absorbing. The band gap of the compound reveals that it is a wide band gap semiconductor. It is to be noted here that the band gap value of the isostructural sulfide analogue, NaGaS₂, is 4.00 eV. Also, there is no difference in the band gap between the anhydrous and hydrated phases, as there is no contribution of Na and its hydration sphere around the Fermi level.¹⁴ The band gap of NaGaSe₂·xH₂O (~3 eV) is very close to that of the isostructural potassium analogue KGaSe₂ (2.6 eV).³² The theoretical band gap calculated using the hybrid

functional (HSE06) is 2.9 eV, which is in very good agreement with the experimental band gap of 3.0 eV. The partial density of states (pDOS) as given in Figure 7b shows the significant contribution of Se 4p orbitals in the valence band and contribution from Ga s states admixed with Se p states in the construction of the conduction band. The contribution of alkali ions to the band gap is negligible. Hence, there exist slight differences in the band gap values of the isostructural analogues AGaSe₂ (A = Na, K, Rb, Cs).^{32–34} The decrease in the band gap by 1 eV from sulfide to selenide analogues is a consequence of the lower electronegativity of Se and greater dispersion of 4p orbitals compared to that of 3p.

Solid-State Ion Exchange. Due to the limited stability of the compound, NaGaSe₂, in pure water, solid-state ion exchange is adopted to evaluate the exchange of Na ions with other monovalent and divalent ions. The PXRD of the solid-state ion-exchanged powder samples (Figure S7) clearly indicates 100% topotactic ion exchange with K⁺ and Rb⁺ ions (Figure S7a), whereas in the case of LiCl and SrCl₂, the layered NaGaSe₂ phase is completely transformed into LiGaSe₂⁴⁰ and SrGa₂Se₄ (Figure S7b).⁴¹ Ion exchange studies also restate the fact that water absorption is unique to the Na-containing layered TlGaQ₂ structure-type, since K- and Rb-containing phases do not absorb water, as also noticed in the case of sulfide analogues.¹⁴ The reaction with LiCl and SrCl₂ created different structure-type materials (see Figure S8), but they preserved the empirical formula and can be regarded as a nontopotactic metathesis reaction. Therefore, in principle, it is possible to create altogether new phases including metastable phases with different monovalent and divalent ions using moderate-temperature solid-state ion exchange.

Impedance Studies. The effect of water intercalation on the ionic conductivity of NaGaSe₂ was examined using electrochemical impedance spectroscopy. The Nyquist plots for hydrated and anhydrous compounds are shown in Figures 8 and S9, which consist of a high-frequency semicircle and a

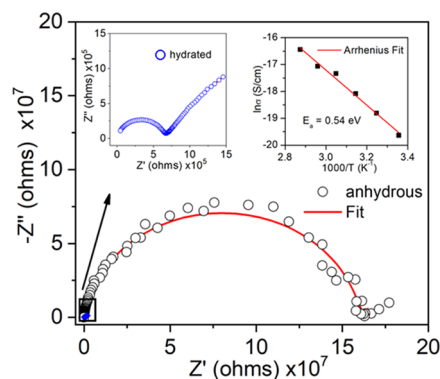


Figure 8. Nyquist plots for room temperature ionic conductivity of anhydrous and hydrated NaGaSe₂. The inset shows the activation energy calculated by Arrhenius fitting from the experimentally measured ionic conductivity versus temperature for the anhydrous NaGaSe₂.

low-frequency tail corresponding to the bulk resistance and charge accumulation at the blocking electrodes. The equivalent circuit used and the related fitting parameters for room temperature ionic conductivity are detailed in the Supporting Information (Figure S10). Ionic conductivity is calculated using the bulk resistance extracted from the complex impedance plots. The activation energies are calculated using

$\sigma_T = \sigma_0 \exp(-E_a/k_B T)$, where σ_T is the ionic conductivity, σ_0 is a pre-exponential factor, T is the absolute temperature, and k_B is the Boltzmann constant. The room temperature ionic conductivity of anhydrous NaGaSe₂ is 2.98×10^{-6} mS/cm with an activation energy of 0.54 eV. Under similar conditions, the hydrated NaGaSe₂ ($d = 9.06$ Å phase) yields a room temperature ionic conductivity of 5.9×10^{-4} mS/cm, which is 2 orders of magnitude higher than that of the anhydrous sample. The activation energy (0.39 eV) for the hydrated phase is also lower than that of the anhydrous phase (Figure S9, inset). The increase in the ionic conductivity in the hydrated phase compared to that of the anhydrous phase can be attributed to the increase in the interlayer distance due to water intercalation, which helps in better diffusion of Na⁺ ions in the lattice. A similar observation was made in the isostructural sulfide analogue NaGaS₂, which displayed a 40 times increase in the ionic conductivity upon water intercalation.¹⁴ However, the increase in ionic conductivity upon water intercalation is much higher in the selenide analogue ($\times 197$) compared to that of sulfide, which could be due to the higher polarizability of selenium.

Vapor Sorption Study. A vapor sorption study has been performed to evaluate the selectivity of H₂O molecule sorption compared to that of other common solvent molecules. Figure 9

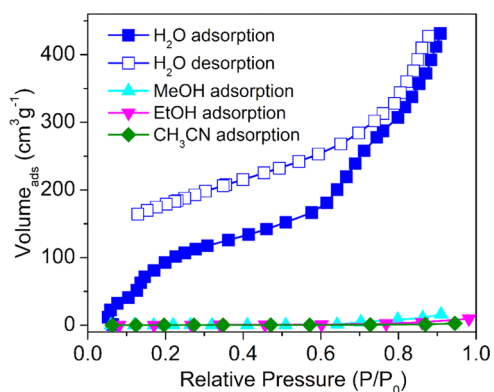


Figure 9. Solvent adsorption profiles of NaGaSe₂ with H₂O, MeOH, EtOH, and CH₃CN at 298 K. P_0 is the saturated vapor pressure of the adsorbates at the measurement temperature.

shows the sorption isotherms of NaGaSe₂ for H₂O, MeOH, EtOH, and CH₃CN vapors. It is clear from the sorption isotherms that NaGaSe₂ is highly selective toward H₂O uptake. A maximum amount of 431 cm³/g water which is equivalent to 6 molecules/formula unit can be absorbed at a relative pressure, P/P_0 , of 0.9. Under the same relative pressure, the adsorption of other solvent molecules is almost negligible. The desorption process of water vapor ends at 169 cm³/g at $P/P_0 = 0.12$, which is equivalent to ~ 2.2 water molecules/formula unit, thus showing a hysteresis between adsorption and desorption processes. This also reiterates the fact that NaGaSe₂ can intercalate ~ 2 molecules of water, NaGaSe₂ $\cdot x$ H₂O ($x \sim 2$), that are tightly bound with interlayer Na ions and cannot be simply desorbed unless thermally activated. Therefore, the number of water molecules in the completely hydrated phase ($d = 10.59$ Å) is roughly equivalent to 2. A similar observation was also made in the case of the sulfide analogue; however, in this case, x in NaGaS₂ $\cdot x$ H₂O is ~ 1 . The nature of water vapor sorption is found to be similar to that of the isostructural phase, NaGaS₂,¹⁴ i.e., type II isotherm with indefinite

multilayer formation of water. The selective absorption of water originates from the negative enthalpy of the hydration reaction of Na⁺ with water and subsequent trapping of water in the interlayer space. This material is capable of absorbing way more water under high vapor pressure close to saturated water vapor pressure (at P/P_0 of 0.9), and the degree of hydration is a function of the partial water vapor pressure. At this point, we do not know the locations of all the water molecules without the X-ray diffraction information as a function of water uptake. We can speculate that such high water uptake may be due to clustering of water to fulfill the coordination unsaturation of Na⁺ ions akin to those seen in the MOF.⁴² However, for layered materials, it would mean further lattice expansion or even exfoliation. On the other hand, some surface adsorption of water cannot be completely ruled out. The ex situ time-dependent hydration studies also display further absorption of water beyond $x \sim 1$ through further expansion of the interlayer space, as there is emergence of a new line at $d = 10.59$ Å (Figure S4). In addition to our previously reported sulfide analogue,¹⁴ materials with such selective water absorption over other small polar solvent molecules are not very common but have been found in MOFs, carbon composites, and polyoxometallates of molybdenum.^{43–47} However, the selective water uptake over small alcohols as a function of vapor pressure has been found in many MOFs.^{48–50} The ability to preferentially absorb a high amount of water over small alcohols, specifically ethanol molecules, can be useful for bioethanol purification and drying.⁴⁹ The ability of anhydrous NaGaSe₂ to absorb water from the atmosphere can be used to trap water from the environment. However, for such use, the air stability of this material needs to be increased.

CONCLUSIONS

The missing phase in the ternary Na–Ga–Se system NaGaSe₂, isostructural to its sulfide analogue NaGaS₂, has been discovered. The compound has been synthesized for the first time using both stoichiometric and polyselenide flux-based reactions. The material shows a unique property of water absorption from the atmosphere and changes its crystal structure to a hydrated phase, which is distinct from the anhydrous phase. There is a huge expansion of interlayer spacings with the formation of two distinct hydrated phases designated as $d = 9.06$ Å for monohydrate and $d = 10.59$ Å for dihydrate, with the occurrence of stacking faults. This structural transformation is reversible, as the crystalline anhydrous phase can be fully recovered by heating the fully hydrated phase to ~ 300 °C under vacuum. As a consequence of hydration, the ionic conductivity of the hydrated phase is 2 orders of magnitude higher than that of the anhydrous phase. Topotactic and nontopotactic metathesis-type ion exchange can be achieved with metal halides containing monovalent and divalent metal ions. Hydrophilicity of Na ions within the structure makes the absorption process selective to water over other solvent molecules. Absorption-induced changes in the crystal structure and ionic conductivity make this class of materials interesting for both fundamental studies and technological applications.

ASSOCIATED CONTENT

Supporting Information

The Supporting Information is available free of charge at <https://pubs.acs.org/doi/10.1021/acs.inorgchem.2c04237>.

Photographs of crystals before and after TG-DSC samples in a crucible, Na-polyhedra, thermodiffraction, PXRD of ex situ hydration, solid-state ion exchange products, structures of solid-state metathesis reactions, equivalent circuit for impedance measurements, SEM images of the re-exposed thermodiffraction sample, atomic coordinates, isotropic and anisotropic thermal parameters from single-crystal X-ray data, Rietveld-refined parameters, atomic coordinates, isotropic thermal parameters of NaGaSe₂, Na–Se bond lengths from single crystals, and Rietveld-refined data (PDF)

Accession Codes

CCDC 2219740 contains the supplementary crystallographic data for this paper. These data can be obtained free of charge via www.ccdc.cam.ac.uk/data_request/cif, or by emailing data_request@ccdc.cam.ac.uk, or by contacting The Cambridge Crystallographic Data Centre, 12 Union Road, Cambridge CB2 1EZ, UK; fax: +44 1223 336033.

AUTHOR INFORMATION

Corresponding Author

Amitava Choudhury – Department of Chemistry, Missouri University of Science and Technology, Rolla, Missouri 65409, United States; orcid.org/0000-0001-5496-7346; Phone: (573)341-6332; Email: choudhurya@mst.edu

Authors

Srikanth Balijapelly – Department of Chemistry, Missouri University of Science and Technology, Rolla, Missouri 65409, United States; orcid.org/0000-0003-2720-8568

Santhoshkumar Sundaramoorthy – Department of Chemistry, Missouri University of Science and Technology, Rolla, Missouri 65409, United States; orcid.org/0000-0001-5037-0016

Dibya Jyoti Mondal – Department of Chemistry, Indian Institute of Science Education and Research, Bhopal 462066, India

Sanjit Konar – Department of Chemistry, Indian Institute of Science Education and Research, Bhopal 462066, India; orcid.org/0000-0002-1584-6258

Nikolay Gerasimchuk – Department of Chemistry, Missouri State University, Springfield, Missouri 65897, United States; orcid.org/0000-0003-4867-6475

Aleksandr Chernatynskiy – Department of Physics, Missouri University of Science and Technology, Rolla, Missouri 65409, United States; orcid.org/0000-0001-7431-7201

Complete contact information is available at:

<https://pubs.acs.org/10.1021/acs.inorgchem.2c04237>

Author Contributions

¹S.B. and S.S. contributed equally.

Notes

The authors declare no competing financial interest.

ACKNOWLEDGMENTS

A. Chernatynskiy, S.B., S.S., and A. Choudhury acknowledge the National Science Foundation (NSF) under Grant Number DMR-1809128 for the funding of this work. The use of the Advanced Photon Source at Argonne National Laboratory was supported by the U.S. Department of Energy, Office of

Science, Office of Basic Energy Sciences, under Contract No. DE-AC02-06CH11357.

REFERENCES

- (1) Suzuki, M.; Wada, N.; Hines, D. R.; Whittingham, M. S. Hydration States and Phase Transitions in Vermiculite Intercalation Compounds. *Phys. Rev. B* **1987**, *36*, 2844–2851.
- (2) Jeevanandam, P.; Vasudevan, S. Conductivity and Dielectric Response in the Ion-Exchange Intercalated Mono- and Double-Layer Hydrates Cd_{0.75}PS₃Na_{0.5}(H₂O)_y, y = 1, 2. *J. Phys. Chem. B* **1998**, *102*, 3082–3089.
- (3) Jin, R.; Sales, B. C.; Khalifah, P.; Mandrus, D. Observation of Bulk Superconductivity in Na_xCoO₂. YH₂O and Na_xCoO₂. YD₂O Powder and Single Crystals. *Phys. Rev. Lett.* **2003**, *91*, No. 217001.
- (4) Hatz, A.-K.; Moudrakovski, I.; Bette, S.; Terban, M. W.; Etter, M.; Joos, M.; Vargas-Barbosa, N. M.; Dinnebier, R. E.; Lotsch, B. Fast Water-Assisted Lithium Ion Conduction in Restacked Lithium Tin Sulfide Nanosheets. *Chem. Mater.* **2021**, *33*, 7337–7349.
- (5) Mähler, J.; Persson, I. A Study of the Hydration of the Alkali Metal Ions in Aqueous Solution. *Inorg. Chem.* **2012**, *51*, 425–438.
- (6) Clement, R. A Novel Route to Intercalation into Layered MnPS₃. *J. Chem. Soc., Chem. Commun.* **1980**, 647.
- (7) Whittingham, M. S. Transport Properties of the Mineral Vermiculite. *Solid State Ionics* **1989**, *32–33*, 344–349.
- (8) Kuhn, A.; Holzmann, T.; Nuss, J.; Lotsch, B. A Facile Wet Chemistry Approach towards Unilamellar Tin Sulfide Nanosheets from Li₄xSn_{1-x}S₂ Solid Solutions. *J. Mater. Chem. A* **2014**, *2*, 6100–6106.
- (9) Takano, A.; Oikawa, I.; Kamegawa, A.; Takamura, H. Enhancement of the Lithium-Ion Conductivity of LiBH₄ by Hydration. *Solid State Ionics* **2016**, *285*, 47–50.
- (10) Maraqah, H.; Li, J.; Whittingham, M. S. The Ionic Conductivity of Hydrogen Vermiculite. *J. Electrochem. Soc.* **1991**, *138*, L61–L63.
- (11) Whittingham, M. S. Hydrogen Motion in Oxides: From Insulators to Bronzes. *Solid State Ionics* **2004**, *168*, 255–263.
- (12) Joos, M.; Schneider, C.; Münchinger, A.; Moudrakovski, I.; Usiskin, R.; Maier, J.; Lotsch, B. V. Impact of Hydration on Ion Transport in Li₂Sn₂S₅·xH₂O. *J. Mater. Chem. A* **2021**, *9*, 16532–16544.
- (13) Klepov, V. V.; Berseneva, A. A.; Pace, K. A.; Kocevski, V.; Sun, M.; Qiu, P.; Wang, H.; Chen, F.; Besmann, T. M.; Loye, H. NaGaS₂: An Elusive Layered Compound with Dynamic Water Absorption and Wide-Ranging Ion-Exchange Properties. *Angew. Chem., Int. Ed.* **2020**, *59*, 10836–10841.
- (14) Adhikary, A.; Yaghoobnejad, H.; Sandineni, P.; Balijapelly, S.; Mohapatra, S.; Khatua, S.; Konar, S.; Gerasimchuk, N.; Chernatynskiy, A.; Choudhury, A. Unusual Atmospheric Water Trapping and Water Induced Reversible Restacking of 2D Gallium Sulfide Layers in NaGaS₂ Formed by Supertetrahedral Building Unit. *Chem. Mater.* **2020**, *32*, 5589–5603.
- (15) Berseneva, A. A.; Klepov, V.; Pal, K.; Seeley, K.; Koury, D.; Schaeperkoetter, J.; Wright, J. T.; Misture, S. T.; Kanatzidis, M. G.; Wolverton, C.; Gelis, A.; zur Loye, H.-C. Transuranium Sulfide via the Boron Chalcogen Mixture Method and Reversible Water Uptake in the NaCuTS₃ Family. *J. Am. Chem. Soc.* **2022**, *144*, 13773–13786.
- (16) Kamaya, N.; Homma, K.; Yamakawa, Y.; Hirayama, M.; Kanno, R.; Yonemura, M.; Kamiyama, T.; Kato, Y.; Hama, S.; Kawamoto, K.; Mitsui, A. A Lithium Superionic Conductor. *Nat. Mater.* **2011**, *10*, 682–686.
- (17) Seino, Y.; Ota, T.; Takada, K.; Hayashi, A.; Tatsumisago, M. A Sulphide Lithium Super Ion Conductor Is Superior to Liquid Ion Conductors for Use in Rechargeable Batteries. *Energy Environ. Sci.* **2014**, *7*, 627–631.
- (18) Richards, W. D.; Tsujimura, T.; Miara, L. J.; Wang, Y.; Kim, J. C.; Ong, S. P.; Uechi, I.; Suzuki, N.; Ceder, G. Design and Synthesis of the Superionic Conductor Na₁₀SnP₂S₁₂. *Nat. Commun.* **2016**, *7*, No. 11009.

- (19) Hayashi, A.; Noi, K.; Sakuda, A.; Tatsumisago, M. Superionic Glass-Ceramic Electrolytes for Room-Temperature Rechargeable Sodium Batteries. *Nat. Commun.* **2012**, *3*, No. 856.
- (20) Schewe-Miller, I. Metallreiche Hauptgruppenmetall-Chalkogenverbindungen: Synthese, Strukturen Und Eigenschaften, Dissertation, Max-Planck-Institute, 1990.
- (21) Kubelka, P.; Munk, F. Ein Beitrag Zur Optik Der Farbanstriche. *Z. Tech. Phys.* **1931**, *12*, 593–601.
- (22) Kresse, G.; Hafner, J. Ab Initio Molecular Dynamics for Liquid Metals. *Phys. Rev. B* **1993**, *47*, 558–561.
- (23) Kresse, G.; Furthmüller, J. Efficiency of Ab-Initio Total Energy Calculations for Metals and Semiconductors Using a Plane-Wave Basis Set. *Comput. Mater. Sci.* **1996**, *6*, 15–50.
- (24) Kresse, G.; Furthmüller, J. Efficient Iterative Schemes for Ab Initio Total-Energy Calculations Using a Plane-Wave Basis Set. *Phys. Rev. B* **1996**, *54*, 11169–11186.
- (25) Kresse, G.; Joubert, D. From Ultrasoft Pseudopotentials to the Projector Augmented-Wave Method. *Phys. Rev. B* **1999**, *59*, 1758–1775.
- (26) Krukau, A. V.; Vydrov, O. A.; Izmaylov, A. F.; Scuseria, G. E. Influence of the Exchange Screening Parameter on the Performance of Screened Hybrid Functionals. *J. Chem. Phys.* **2006**, *125*, No. 224106.
- (27) Monkhorst, H. J.; Pack, J. D. Special Points for Brillouin-Zone Integrations. *Phys. Rev. B* **1976**, *13*, 5188–5192.
- (28) Müller, D.; Hahn, H. Untersuchungen über Ternäre Chalkogenide. XXIV. Zur Struktur Des $TlGaSe_2$. *Z. Anorg. Allg. Chem.* **1978**, *438*, 258–272.
- (29) Lemoine, P.; Carré, D.; Guittard, M. Structure Du Sulfure de Gallium et de Potassium, $KGaS_2$. *Acta Crystallogr., Sect. C* **1984**, *40*, 910–912.
- (30) Kim, J.; Hughbanks, T. Synthesis and Structures of Ternary Chalcogenides of Aluminum and Gallium with Stacking Faults: KMQ_2 ($M = Al, Ga; Q = Se, Te$). *J. Solid State Chem.* **2000**, *149*, 242–251.
- (31) Kumari, A.; Vidyasagar, K. Rubidium Thiogallate. *Acta Crystallogr., Sect. E* **2005**, *61*, i193–i195.
- (32) Feng, K.; Mei, D.; Bai, L.; Lin, Z.; Yao, J.; Wu, Y. Synthesis, Structure, Physical Properties, and Electronic Structure of $KGaSe_2$. *Solid State Sci.* **2012**, *14*, 1152–1156.
- (33) Friedrich, D.; Schlosser, M.; Pfitzner, A. Synthesis, Crystal Structure, and Physical Properties of Two Polymorphs of $CsGaSe_2$, and High-Temperature X-Ray Diffraction Study of the Phase Transition Kinetics. *Cryst. Growth Des.* **2016**, *16*, 3983–3992.
- (34) Friedrich, D.; Schlosser, M.; Pfitzner, A. Synthesis and Structural Characterization of the Layered Selenogallate $RbGaSe_2$. *Z. Anorg. Allg. Chem.* **2017**, *643*, 1589–1592.
- (35) Friedrich, D.; Schlosser, M.; Weihrich, R.; Pfitzner, A. Polymorphism of $CsGaS_2$ – Structural Characterization of a New Two-Dimensional Polymorph and Study of the Phase-Transition Kinetics. *Inorg. Chem. Front.* **2017**, *4*, 393–400.
- (36) Verger, L.; Trébosc, J.; Baptiste, B.; Furet, E.; Dénoue, K.; Zhang, J.; Cheviré, F.; le Coq, D.; Calvez, L.; Lafon, O.; Hernandez, O. Mechanochemical Synthesis and Study of the Local Structure of $NaGaS_2$ Glass and Glass–Ceramics. *Inorg. Chem.* **2022**, *61*, 18476–18485.
- (37) Leal-Gonzalez, J.; Melibary, S. A.; Smith, A. J. Structure of Lithium Gallium Sulfide, $LiGaS_2$. *Acta Crystallogr., Sect. C* **1990**, *46*, 2017–2019.
- (38) Isaenko, L.; Vasilyeva, I.; Merkulov, A.; Yelissev, A.; Lobanov, S. Growth of New Nonlinear Crystals $LiMX_2$ ($M = Al, In, Ga; X = S, Se, Te$) for the Mid-IR Optics. *J. Cryst. Growth* **2005**, *275*, 217–223.
- (39) Li, X.; Liang, F.; Liu, T.; Li, H. Na_2GaS_2Cl : A New Sodium-Rich Chalcogenide with Two-Dimensional $[GaS_2]_{\infty}$ Layers and Wide Interlayer Space. *Dalton Trans.* **2021**, *50*, 11167–11172.
- (40) Kuriyama, K.; Nozaki, T. Single-crystal Growth and Characterization of $LiGaSe_2$. *J. Appl. Phys.* **1981**, *52*, 6441–6443.
- (41) Klee, W.; Schafer, H. Die Struktur Des $SrGa_2Se_4$, Eine Neue Besetzungsvariante Des $TlSe$ -Typs. *Z. Anorg. Allg. Chem.* **1983**, *499*, 145–152.
- (42) Wu, H.; Gong, Q.; Olson, D. H.; Li, J. Commensurate Adsorption of Hydrocarbons and Alcohols in Microporous Metal Organic Frameworks. *Chem. Rev.* **2012**, *112*, 836–868.
- (43) Uchida, S.; Mizuno, N. Zeotype Ionic Crystal of $Cs_3[Cr_3O(OOCH)_6(H_2O)_3][\alpha-CoW_{12}O_{40}] \cdot 7.5H_2O$ with Shape-Selective Adsorption of Water. *J. Am. Chem. Soc.* **2004**, *126*, 1602–1603.
- (44) Chen, B.; Ji, Y.; Xue, M.; Fronczek, F. R.; Hurtado, E. J.; Mondal, J. U.; Liang, C.; Dai, S. Metal–Organic Framework with Rationally Tuned Micropores for Selective Adsorption of Water over Methanol. *Inorg. Chem.* **2008**, *47*, 5543–5545.
- (45) Ogasawara, Y.; Uchida, S.; Maruichi, T.; Ishikawa, R.; Shibata, N.; Ikuhara, Y.; Mizuno, N. Cubic Cesium Hydrogen Silicododecatungstate with Anisotropic Morphology and Polyoxometalate Vacancies Exhibiting Selective Water Sorption and Cation-Exchange Properties. *Chem. Mater.* **2013**, *25*, 905–911.
- (46) Plessius, R.; Kromhout, R.; Ramos, A. L. D.; Ferbinteanu, M.; Mittelmeijer-Hazeleger, M. C.; Krishna, R.; Rothenberg, G.; Tanase, S. Highly Selective Water Adsorption in a Lanthanum Metal–Organic Framework. *Chem. – Eur. J.* **2014**, *20*, 7922–7925.
- (47) Di, Z.; Pang, J.; Hu, F.; Wu, M.; Hong, M. An Ultra-Stable Microporous Supramolecular Framework with Highly Selective Adsorption and Separation of Water over Ethanol. *Nano Res.* **2021**, *14*, 2584–2588.
- (48) Guan, L. Z.; Patiño, J.; Cuadrado-Collados, C.; Tamayo, A.; Gutiérrez, M. C.; Ferrer, M. L.; Silvestre-Albero, J.; del Monte, F. Carbon–GO Composites with Preferential Water versus Ethanol Uptake. *ACS Appl. Mater. Interfaces* **2019**, *11*, 24493–24503.
- (49) Shigematsu, A.; Yamada, T.; Kitagawa, H. Selective Separation of Water, Methanol, and Ethanol by a Porous Coordination Polymer Built with a Flexible Tetrahedral Ligand. *J. Am. Chem. Soc.* **2012**, *134*, 13145–13147.
- (50) Hu, J.; Xu, Y.; Zhang, D.; Chen, B.; Lin, Z.; Hu, C. A Highly Symmetric Ionic Crystal Constructed by Polyoxoniobates and Cobalt Complexes for Preferential Water Uptake over Alcohols. *Inorg. Chem.* **2017**, *56*, 10844–10847.

Recommended by ACS

$Ba_{1.09}Pb_{0.91}Be_2(BO_3)_2F_2$: The First Pb-Containing Beryllium Borate Fluoride with Trigonal Prismatic PbO_6 and 2D $[Be_3B_3O_6F_3]_{\infty}$ Layers

Ruixin Guo, Xiaoyang Wang, et al.

FEBRUARY 20, 2023
INORGANIC CHEMISTRY

READ 

Alignment of Λ -Shaped Basic Building Units to Construct One New $KMoO_3(IO_3)$ Polar Polymorph

Qing Li, Hongping Wu, et al.

FEBRUARY 22, 2023
INORGANIC CHEMISTRY

READ 

Two Mixed-Alkali-Metal Selenates as Short-Wave Ultraviolet Nonlinear-Optical Materials

Qian Yan, Guohong Zou, et al.

MARCH 13, 2023
INORGANIC CHEMISTRY

READ 

d^6 versus d^{10} , Which Is Better for Second Harmonic Generation Susceptibility? A Case Study of $K_2TGe_3Ch_8$ ($T = Fe, Cd; Ch = S, Se$)

Bingheng Ji, Jian Wang, et al.

DECEMBER 27, 2022
INORGANIC CHEMISTRY

READ 

Get More Suggestions >